

Direct Proteomic and High-Resolution Microscopy Biopsy Analysis Identifies Distinct Ventricular Fates in Severe Aortic Stenosis

Full Length Article

Brandenburg *et al.* Proteomic profiling of severe aortic stenosis.

Sören Brandenburg^{a, b, c, d, *}, Lena Drews^b, Hanne-Lea Schönberger^b, Christoph F. Jacob^{a, b}, Nora Josefine Paulke^b, Bo E. Beuthner^{a, c}, Rodi Topci^a, Tobias Kohl^{a, b}, Lisa Neuenroth^e, Ingo Kutschka^f, Henning Urlaub^{e, g, h}, Fabian Kückⁱ, Andreas Leha^{c, i}, Tim Friede^{c, i}, Tim Seidler^{a, c}, Claudius Jacobshagen^j, Karl Toischer^{a, c, d, k}, Miriam Puls^{a, c}, Gerd Hasenfuß^{a, b, c, d, k}, Christof Lenz^{d, e, g, k, l}, Stephan E. Lehnart^{a, b, c, d, h, k, l, *}

^a Clinic of Cardiology & Pneumology, University Medical Center Göttingen, Germany

^b Cellular Biophysics & Translational Cardiology Section, Heart Research Center Göttingen, University Medical Center Göttingen, Germany

^c DZHK (German Centre for Cardiovascular Research), Partner Site Göttingen, Germany

^d Collaborative Research Center SFB1002 “Modulatory Units in Heart Failure”, University of Göttingen, Germany

^e Department of Clinical Chemistry, University Medical Center Göttingen, Germany

^f Clinic of Cardiothoracic & Vascular Surgery, University Medical Center Göttingen, Germany

^g Bioanalytical Mass Spectrometry Group, Max Planck Institute for Multidisciplinary Sciences, Göttingen, Germany

^h Collaborative Research Center SFB1190 “Compartmental Gates and Contact Sites in Cells”, University of Göttingen, Germany

ⁱ Department of Medical Statistics, University Medical Center Göttingen, Germany

^j Department of Cardiology, Intensive Care & Angiology, Vincentius-Diakonissen-Hospital Karlsruhe, Germany

^k Cluster of Excellence "Multiscale Bioimaging: from Molecular Machines to Networks of Excitable Cells" (MBExC), University of Göttingen, Germany

^l Leducq Transatlantic Network of Excellence CURE-PLaN

* Corresponding authors: Sören Brandenburg and Stephan E. Lehnart

University Medical Center Göttingen; Robert-Koch-Str. 42a, 37075 Göttingen, Germany

Tel: +49 551 39-63631

Email: soeren.brandenburg@med.uni-goettingen.de, slehnart@med.uni-goettingen.de

Supplementary information

1. Supplementary methods
2. Supplementary figures and figure legends
3. Supplementary tables

Supplementary Fig. 1. Quantile normalization.

Supplementary Fig. 2. Correlations of technical replicates.

Supplementary Fig. 3. Principal component analysis of DIA-MS data colored by left-ventricular ejection fraction.

Supplementary Fig. 4. ConsensusClusterPlus.

Supplementary Fig. 5. Hierarchical clustering.

Supplementary Fig. 6. Enriched Gene Ontology terms relative to LEF-LG.

Supplementary Fig. 7. Comorbidities coronary artery disease and atrial fibrillation in AS.

Supplementary Fig. 8. Overrepresented KEGG pathways in clusters i-iv) of Fig. 1C.

Supplementary Fig. 9. Correlation analysis of 160 differentially abundant proteins with left-ventricular echocardiography parameters.

Supplementary Fig. 10. Lipofuscin aggregates are increased in aortic stenosis-affected left-ventricular cardiomyocytes.

Supplementary Fig. 11. The periodicity of transversal ryanodine receptor type 2 (RyR2) cluster striations is strongly impaired in LEF-HG and LEF-LG.

Supplementary Table 1. Clinical characteristics and pre-interventional echocardiographic parameters from patients with left-ventricular biopsy samples analyzed by DIA-MS and superresolution STED microscopy.

Supplementary Table 2. Clinical characteristics and pre-interventional echocardiographic parameters from patients with proteomically analyzed left-ventricular biopsy samples for DIA-MS.

Supplementary Table 3. Clinical characteristics and pre-interventional echocardiographic parameters from patients with left-ventricular biopsy samples analyzed by superresolution STED microscopy.

Supplementary Table 4. Hierarchical clustering.

Methods

Mass spectrometry-based proteome profiling

Tissue lysis and sample processing

Human LV biopsies (4-7 mg) were lysed in a barocycler (model 2320 EXT, Pressure Biosciences) using an 8 mM urea buffer supplemented with enzyme and phosphatase inhibitors and 60 pressure cycles (45 kpsi, 50 s pressure + 10 s release, 33°C). Reduction and alkylation were performed at 30°C with 10 mM tris(2-carboxyethyl)phosphin and 40 mM iodoacetamide for 30 min. Protein concentrations were estimated based on tissue volume to preserve sample amounts. Tryptic digestion was achieved after dilution using a 1:20 enzyme-to-substrate ratio and 90 pressure cycles (20 kpsi, 50+10 s, 37°C). Peptide samples were desalted on reversed phase C18 material and dried in a vacuum concentrator for further analysis [1].

Label-free quantitative mass spectrometry

For generation of a peptide library, equal amount aliquots from each sample were pooled to a total amount of 150 µg, dried in a vacuum concentrator and resuspended in 0.1% TFA. The pool was then separated into 14 fractions by reversed phase chromatography (1.0 mm ID x 150 mm, Hypersil Gold C18 aq, 5 µm, Thermo Fisher Scientific) using a 5-40% acetonitrile/0.01M ammonium hydroxide (pH 8.0) at 200 µl min⁻¹ and a staggered pooling scheme (1+15+29) [2]. All samples were spiked with a synthetic peptide standard used for retention time alignment (iRT Standard, Biognosys).

Protein digests were analyzed on a nanoflow chromatography system (Eksigent nanoLC425) hyphenated to a hybrid triple quadrupole-TOF mass spectrometer (TripleTOF 5600+) equipped with a Nanospray III ion source (Ionspray Voltage 2400 V, Interface Heater Temperature 150°C, Sheath Gas Setting 12) and controlled by Analyst TF 1.7.1 software build 1163 (all AB Sciex). In brief, peptides were dissolved in loading buffer (2% acetonitrile, 0.1% formic acid in water) to a concentration of 0.3 µg/µl. Concentrations were adjusted by short LC/MS/MS

test injections of stock solutions and comparison of the observed Total Ion Chromatogram (TIC) areas to injections of a homemade cell lysate tryptic digest standard of known concentration.

For each analysis 1.5 μg of digested protein were enriched on a micro pillar array trapping column (1 cm length, μPac 5 μm , PharmaFluidics) and separated on an analytical micro pillar array column (200 cm, μPac 2.5 μm , PharmaFluidics) using a 120 min linear gradient of 5-40 % acetonitrile/0.1% formic acid (v:v) at 450 nl min⁻¹.

Qualitative LC/MS/MS analysis was performed using a Top20 data-dependent acquisition (DDA) method with a MS survey scan of m/z 350–1250 accumulated for 250 ms at a resolution of 30,000 full width at half maximum (FWHM). MS/MS scans of m/z 180–1600 were accumulated for 85 ms at a resolution of 17,500 FWHM and a precursor isolation width of 0.7 FWHM, resulting in a total cycle time of 2.0 s. Precursors above a threshold MS intensity of 125 cps with charge states 2+, 3+, and 4+ were selected for MS/MS. The dynamic exclusion time was set to 45 s. MS/MS activation was achieved by CID using nitrogen as a collision gas and the manufacturer's default rolling collision energy settings. Four technical replicates per reversed phase fraction were analyzed to construct a spectral library.

For quantitative data-independent acquisition (DIA)-MS, MS/MS data were acquired using 65 variable size windows [3, 4] across the 400.0-1047.5 m/z range, which contained 95% of peptide precursors identified in the DDA experiment above (**Online Source 13**). Fragments were produced using rolling collision energy settings for charge state 2+, and fragments acquired over an m/z range of 350–1400 for 40 ms per segment. Including a 100 ms survey scan, this resulted in an overall cycle time of 2.97 s. Two replicate injections were acquired for each biological sample.

Data analysis

Protein identification was achieved using ProteinPilot Software version 5.0 build 4769 (AB Sciex) at “thorough” settings. The combined qualitative runs were searched against the UniProtKB Homo sapiens reference proteome (revision 04-2017, 93,069 entries) augmented with a set of 52 known common laboratory contaminants to identify 2,951 proteins at a False Discovery Rate (FDR) of 1%.

Spectral library generation and extraction of quantitative data from DIA-MS were achieved in PeakView Software version 2.1 build 11041 (AB Sciex) using the SWATH quantitation microApp version 2.0 build 2003. Following retention time correction using the iRT standard, peak areas were extracted using information from the MS/MS library at an FDR of 1% [5]. The resulting peak areas were summed to peptide and finally protein area values normalized using a Total Area Sums approach to provide quantitative information on 2,273 proteins across all samples, which were used for further statistical analysis.

For further analysis, 111 proteins belonging to the gene ontology term “blood microparticle” were excluded. Among the 2,162 measured proteins there were 9 proteins (P13535, P31946, P49721, J3QT28, C9JIZ6, P54725, E7ERC8, Q5SWX8, and O00487) with quantification values of zero in at least 37 (74%) samples. There were further 70 proteins with quantification values in at most 3 (6%) samples. In the remaining 2083 proteins quantification values were present (> 0) in all samples. In this study the proteomic data was analyzed as is, i.e. these values were set to zero.

Protein quantifications were log-transformed and quantile-normalized between all samples. The quantile normalization was applied to remove global shifts in the quantifications between samples (**Supplementary Fig. 1**). Correlation between the technical replicates was assessed using *Pearson* correlation coefficient (**Supplementary Fig. 2**).

A principal component analysis was conducted on all samples, and potentially outlying samples were identified (**Fig. 1B** and **Supplementary Fig. 3**). Hierarchical clustering on differential protein abundance was tested for using limma version 3.40.6 [6] to benefit from Bayesian variance-pooling. The hierarchical structure in the data induced by the technical replication of the biological replicates was accounted for by using the common correlation method suggested in [7]. Results from the ANOVA-type tests across all groups are presented, and pairwise contrast test results are visualized in volcano plots. Using z-scores of the significantly differential proteins (from the ANOVA-type test) hierarchical clustering using Euclidian distance and complete linkage was applied to find clusters among the proteins as well as among the samples. To assess the number of clusters present among the samples, consensus clusters were constructed for clusterings into 2-15 clusters and the consensus matrices were plotted for visual inspection as well as analyzed regarding the distribution of their entries (**Supplementary Fig. 4**) [8]. Additionally, the number of clusters was assessed using different statistics (frey, mcclain, cindex, silhouette, dunn, kl, ch, hartigan, db, duda, pseudot2, beale, ratkowsky, ball, ptbiserial, gap, gamma, gplus, tau, hubert, sdindex, dindex, and sdbw), which were also calculated on these clusterings into 2-15 clusters (**Supplementary Fig. 5, Supplementary Table 4**). Functional enrichment towards gene ontology terms was tested for using one-sided Fisher tests as overrepresentation tests as implemented in clusterProfiler version 3.12.0 [9]. Protein wise tests as well as gene set wise tests were corrected for multiple testing using Benjamini-Hochberg to control the false discovery rate. The significance level was set to $\alpha = 0.05$. Analyses on the proteomics data were performed with the Statistical Computing Software R version 3.6.1 if not stated otherwise.

Microscopic and nanoscopic imaging

Histology and (immuno-)fluorescence labeling

LV biopsies were fixed in 4% PFA (Roti-Histofix 4%, Carl Roth), embedded in paraffin and cut into 5 μm thick histological sections. After deparaffinization and rehydration, sections were stained with hematoxylin/eosin (HE, Sigma Aldrich) using standard techniques. Finally, samples were dehydrated, transferred to Xylol, and mounted with Cytoseal 60 (Thermo Fisher Scientific). Imaging was performed with a Zeiss Axio Vert.A1 inverted microscope. Analyses of myocyte cross section area and maximal diameter were performed in Fiji (<https://imagej.net/Fiji>).

For (immuno-)fluorescence labeling of deparaffinized and rehydrated histological sections, antigens were unmasked in 10 M sodium-citrate buffer prior to antibody or WGA incubation. Next, samples were blocked and permeabilized with 4% BSA and 0.1% Triton-X100 in PBS for 1h. Primary antibodies were diluted in PBS containing 4% BSA and incubated with samples overnight in a wet chamber at 20°C using the following dilutions: anti-RyR2 1:100 (HPA020028, Sigma Aldrich), anti-CAV3 1:250 (610421, BD Biosciences). After washing in PBS, samples were incubated with secondary antibodies for 2 h at 20°C: goat anti-rabbit STAR 635P 1:300 (2-0012-007-2, Abberior), goat anti-mouse STAR 580 1:300 (2-0002-007-5, Abberior), and goat anti-mouse STAR 580 1:300 (2-0002-005-1, Abberior). Unconjugated wheat germ agglutinin (WGA, VES-L-1020-10, Biozol) was labeled by NHS esters (STAR 488, 1-0101-006-9; and STAR 580, 1-0101-005-2, Abberior) according to customized protocols [10], and was incubated at ~10 μM with samples in blocking buffer in combination with the secondary antibodies. Following washing steps, coverslips were mounted with ProLong Gold Antifade mountant (Thermo Fisher Scientific).

Lipofuscin autofluorescence imaging

Autofluorescence of perinuclear lipofuscin granules in cardiomyocytes was excited at 405 nm with a laser power of 2% and emission detected between 600-740 nm using a Zeiss LSM 710 confocal microscope and an EC Plan-Neofluar 20 x/0.50 M27 objective (pixel size 210 x 210 nm). We used uniform intensity thresholding for all images at an 8-bit grayscale level of 160 to binarize the lipofuscin signals for quantitative analysis in Fiji.

Transverse-axial tubule (TAT) network analysis

Intracellular TAT endomembrane structures in cardiomyocytes were stained in longitudinally oriented biopsy sections by WGA coupled to STAR 488 and acquired using a Leica TCS SP8 microscope and a HC PL APO C2S 100x/1.40 oil objective (excitation 500 nm, emission detection 510-560 nm, laser power 0.4%, pixel size 114 x 114 nm). Intracellular ROIs excluding nuclei were manually selected for membrane structure segmentation according to previously described protocols for Fiji [10, 11].

Superresolution STED microscopy

STED images of fluorescently (immuno-)labeled human LV biopsy sections were acquired with a Leica TCS SP8 laser-scanning microscope and a HC PL APO C2S 100x/1.40 oil objective. The STED imaging workflows were optimized for the STAR 635P and STAR 580 fluorophores: pixel size 16.23 x 16.23 nm, pixel dwell time 400 ns, scanning speed 600 Hz, 32x line averaging, excitation by a white-light laser at 635 and 580 nm, STED depletion at 775 nm, and fluorescence detection between 650-700 nm and 600-630 nm, respectively. 40 nm fluorescent beads (Abberior Nanoparticles red fluorescent 40 nm) were detected with a FWHM of 70.2 ± 6.4 nm ($n = 7$).

STED image analysis

For detailed quantitative RyR2 and CAV3 signal analysis we adapted previously published protocols based on dual-color STED signal segmentation [12]. Intracellular ROIs of left-ventricular myocytes in longitudinal orientation were manually selected for RyR2 + CAV3 costained biopsy samples, while excluding signals at the surface sarcolemma, nuclei or lipofuscin granules. Immunofluorescence signal patterns were binarized by the following Fiji software commands [12], and additional commands were optimized for background subtraction, smoothing and global versus local thresholding (scaling given in “number of pixels”):

RyR2:

```
run("Subtract Background...", "rolling=45");
run("Enhance Local Contrast (CLAHE)", "blocksize=35 histogram=256 maximum=3
mask=*None*");
run("Gaussian Blur...", "sigma=1");
run("Auto Local Threshold", "method=Bernsen radius=20 parameter_1=0
parameter_2=0 white");
```

CAV3 (RyR2 co-staining):

```
run("Subtract Background...", "rolling=45");
run("Enhance Local Contrast (CLAHE)", "blocksize=35 histogram=256 maximum=3
mask=*None*");
run("Gaussian Blur...", "sigma=1");
run("Auto Threshold", "method=Otsu ignore_black white");
```

In addition, CAV3 signals were dilated once adding 1 pixel to edges to identify CAV3-associated (junctional) RyR2 clusters overlapping with CAV3:

```
run("Dilate", "stack");
```

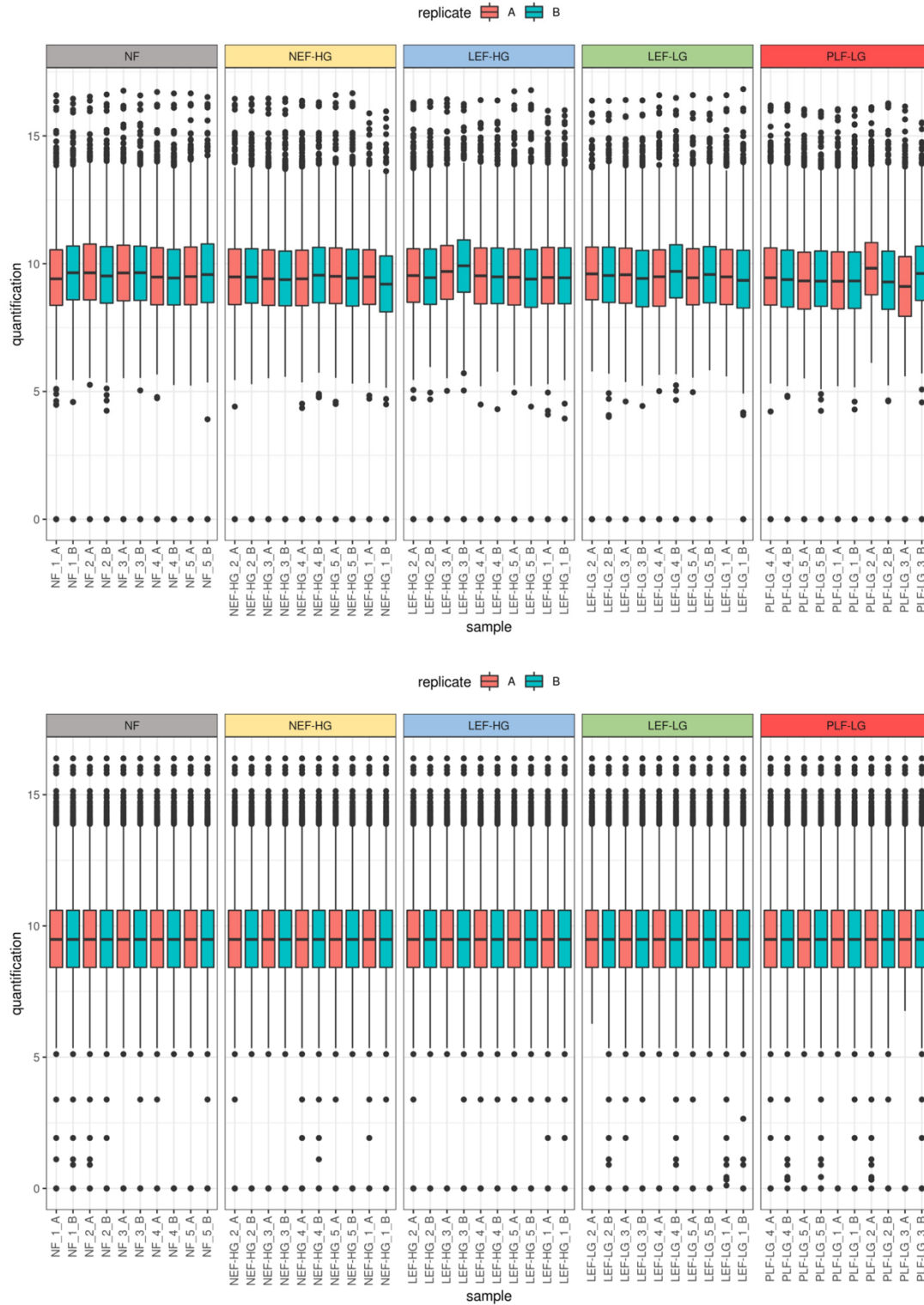
For the analysis of CAV3-associated RyR2 clusters, we accepted RyR2 clusters with partial to complete overlap with CAV3 clusters in binarized images. All signals $\geq 0.001 \mu\text{m}^2$ size up to infinity were considered for cluster analysis. **Fig. 6** in the main manuscript report the calculated signal information (based on the image segmentation steps described above) as signal area fraction, cluster density, CAV3-associated cluster fraction, and CAV3-associated cluster size.

For the analysis of RyR2 cluster configurations, segmented RyR2 images were converted into Euclidian distance maps. RyR2 signals within a nearest-neighbor distance (NND) ≤ 100 nm were summarized into functional inter-cluster assemblies according to the Baddeley *et al.* model of Ca^{2+} release units published previously [13].

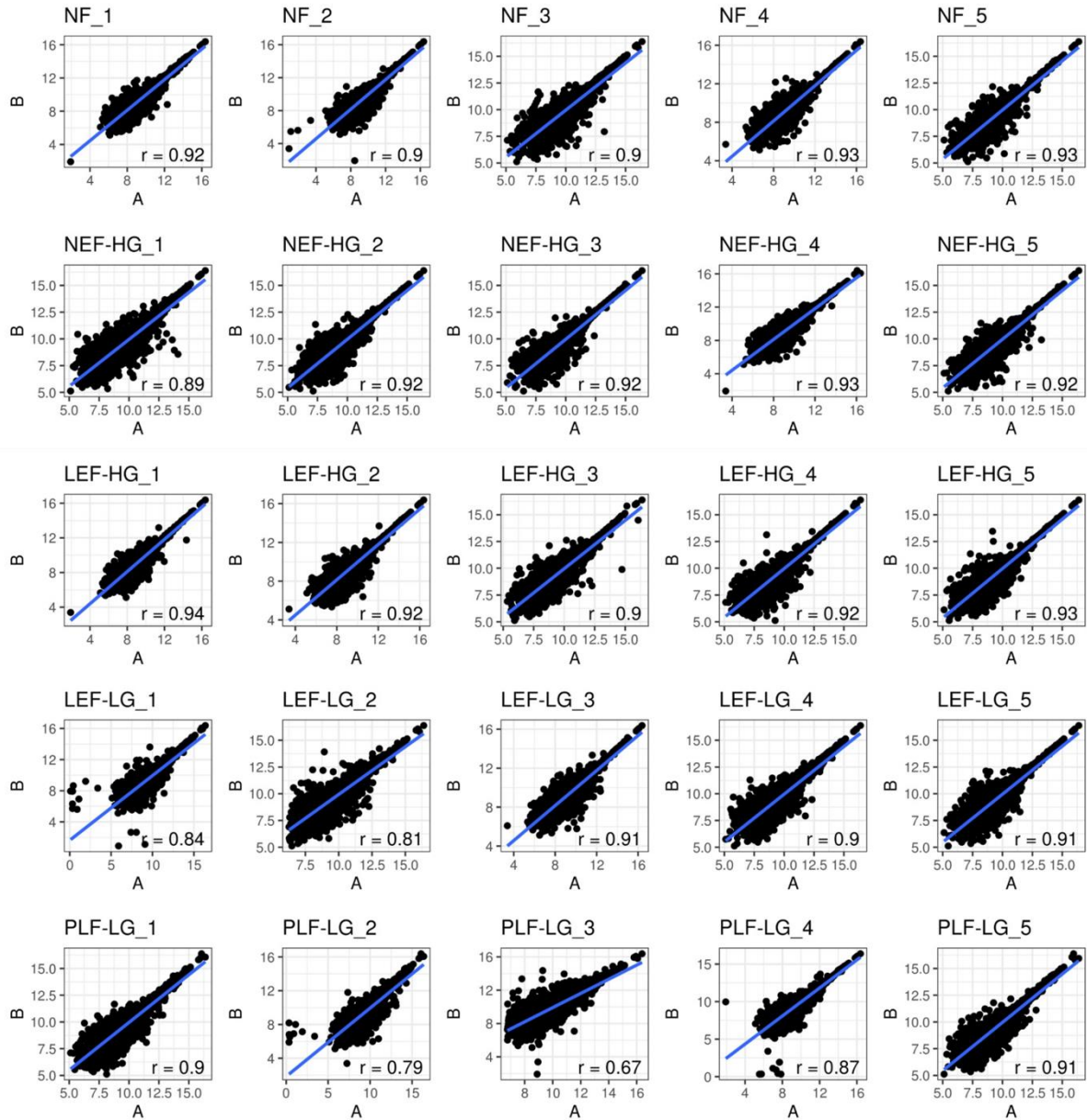
Statistical analysis of imaging data

Data plotting and statistical analyses were performed in GraphPad Prism 7.03, Origin-Pro 8.5G and SPSS Statistics 28.0.1.1. Data were tested for normal distribution and presented as mean \pm SEM unless indicated otherwise. Boxplots indicate the median and the interquartile range, and whiskers represent the 5th and 95th percentiles. In **Fig. 4**, differences between groups were analyzed by one-way ANOVA corrected for multiple comparisons using statistical hypothesis testing (Tukey's test). In **Fig. 5-7**, differences between groups were analyzed by fitting linear mixed models with random intercepts for biological replicates and applying post-hoc Tukey's HSD tests in SPSS Statistics 28.0.1.1. *P* values < 0.05 were considered statistically significant.

For univariate linear regression modeling, we used the Statistical Computing Software R version 3.4.0. In order to consider multiple measurements of the independent variables, we applied the simulation extrapolation (SIMEX) algorithm (R-package SIMEX version 1.8) [14, 15]. The significance level was set to $\alpha = 0.05$.



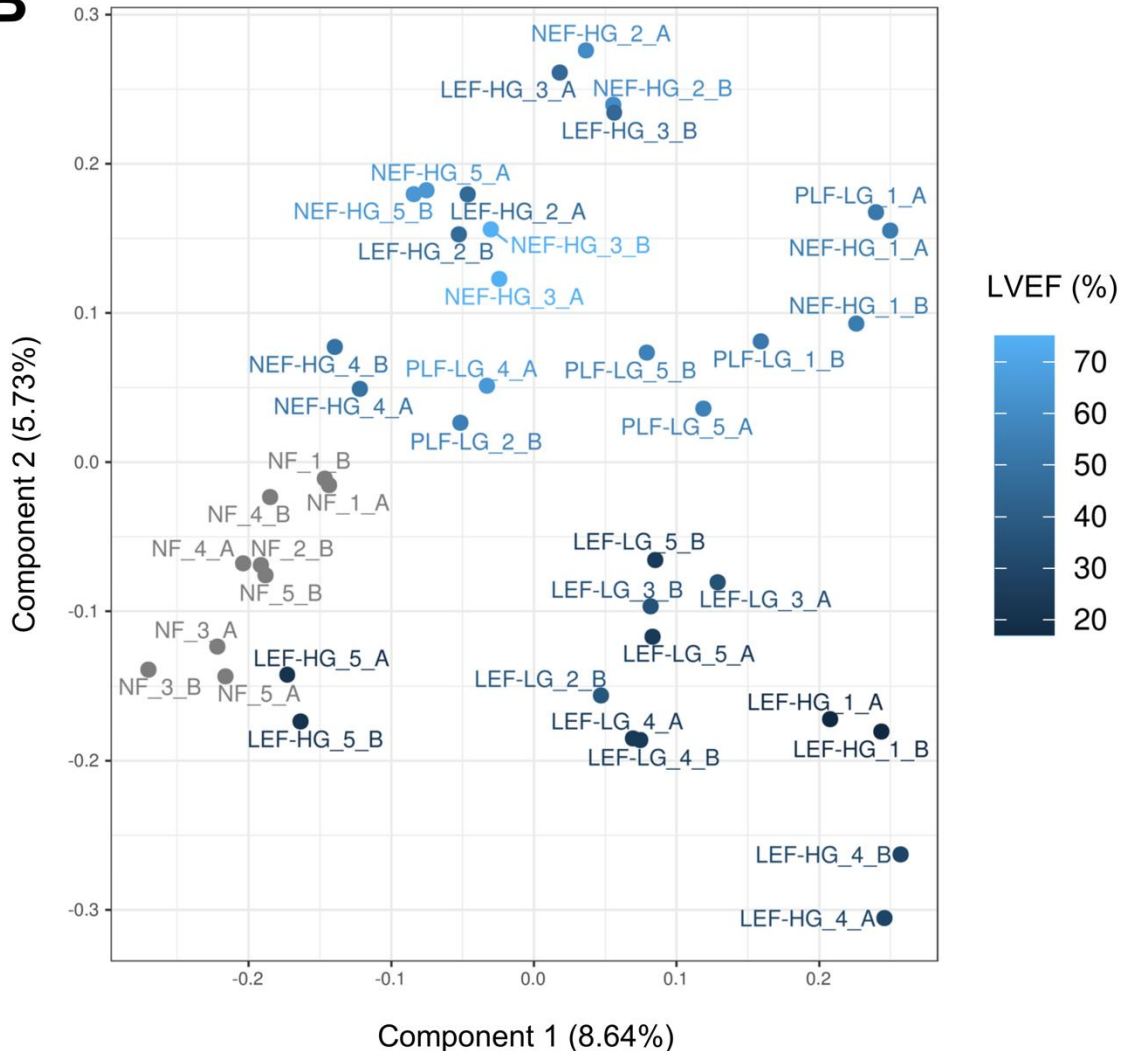
Supplementary Fig. 1. Quantile normalization. Protein quantifications on the log scale (y-axis) by sample and replicate (x-axis) in all groups. (A) Log values prior to, and (B) log values post quantile normalization in boxplots indicating the median and the interquartile range.



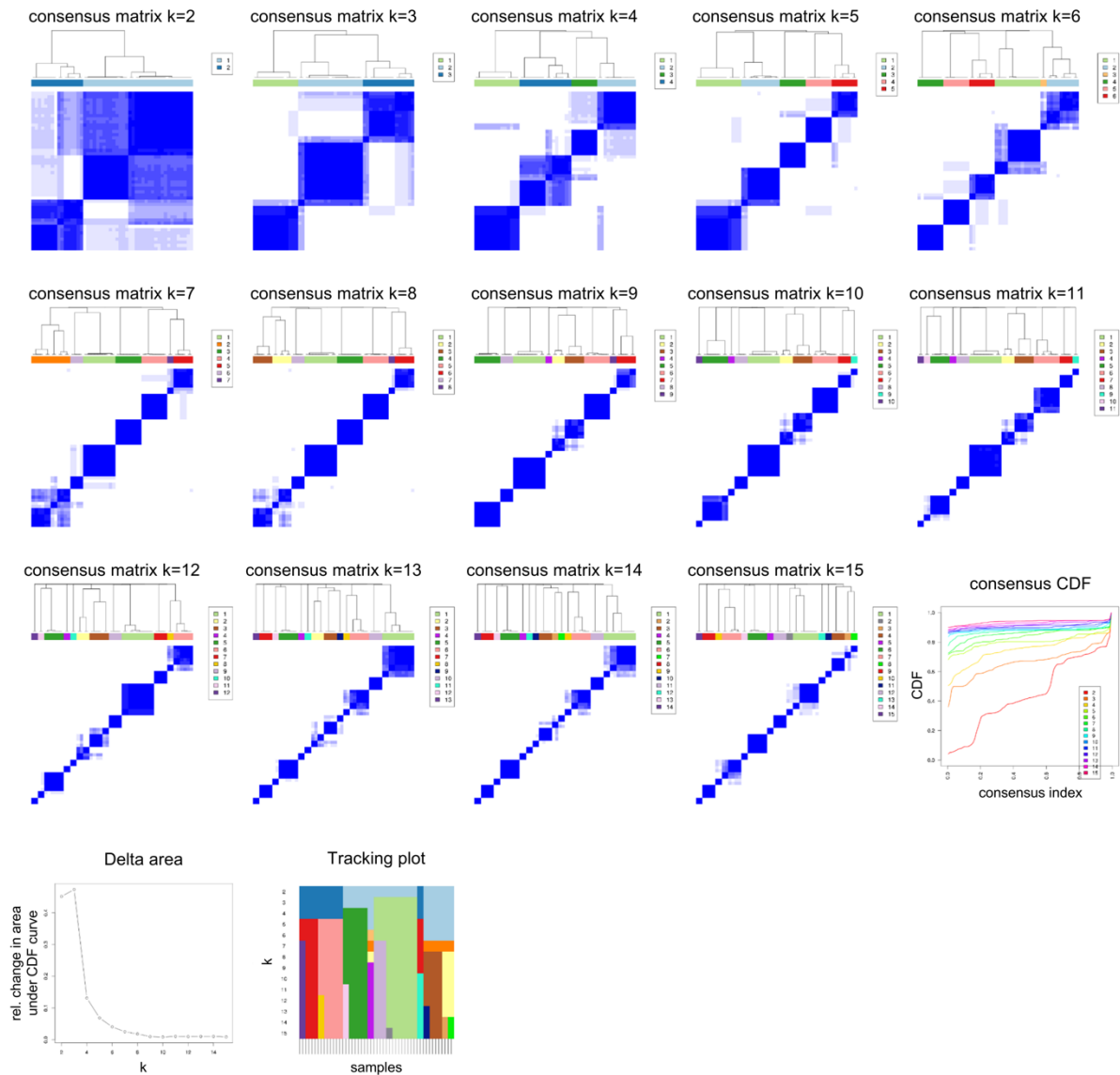
Supplementary Fig. 2. Correlations of technical replicates. Scatterplots showing the protein quantifications between the two technical replicates A and B for each LV patient biopsy and linear regression curves (blue). r , Pearson correlation coefficient.

A

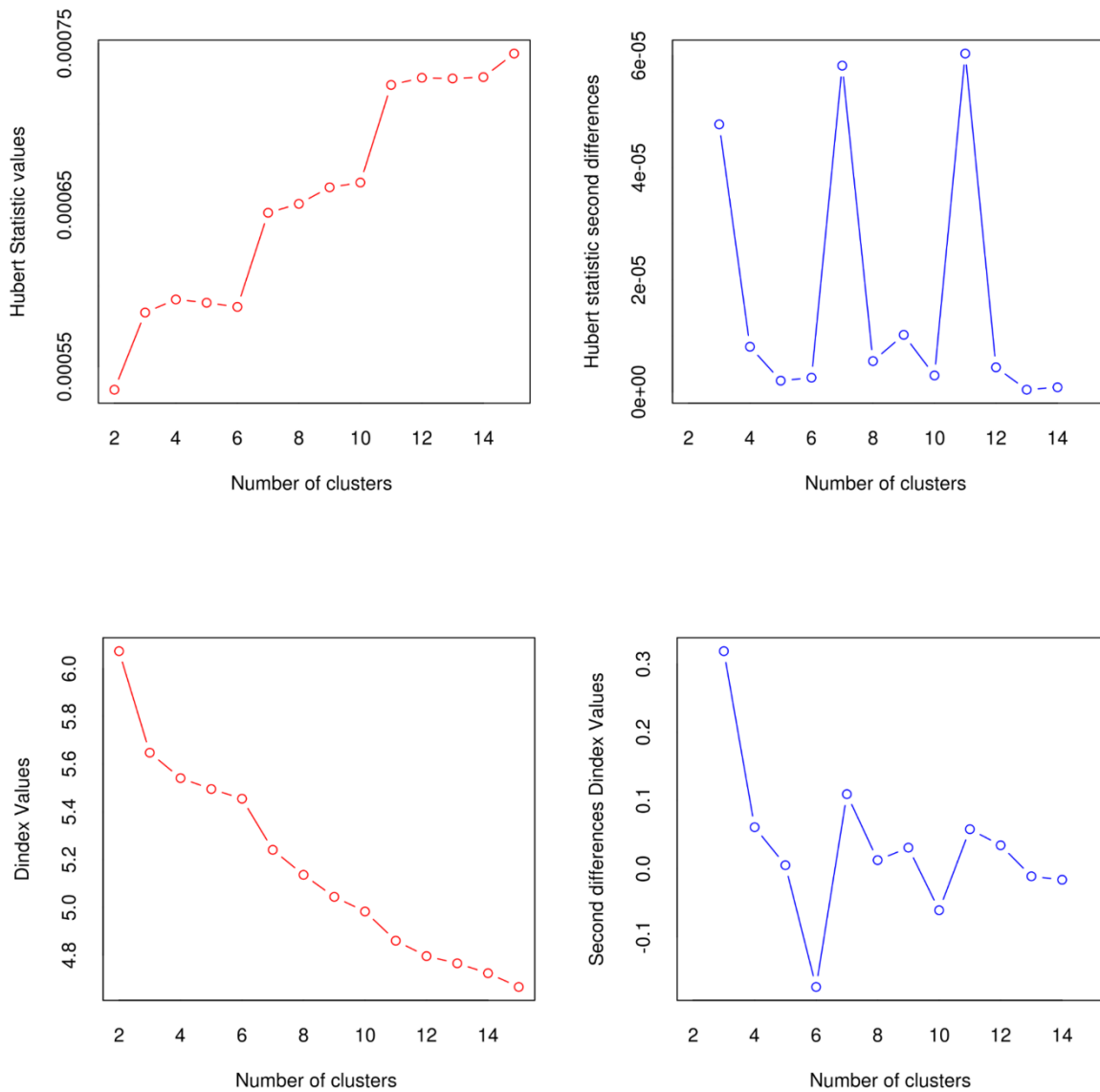
LEF-HG (ID)	1	2	3	4	5
LVEF (%)	17	47	46	30	22

B

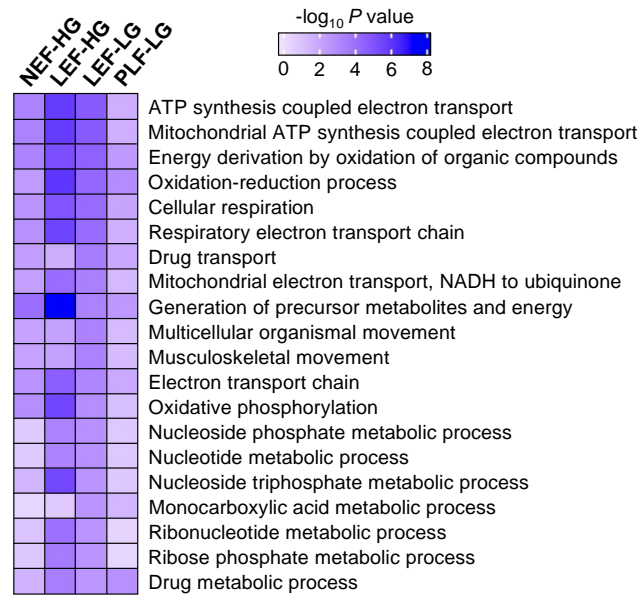
Supplementary Fig. 3. Principal component analysis of DIA-MS data colored by left-ventricular ejection fraction. (A) Left-ventricular ejection fraction (LVEF) data for the five LEF-HG biopsies. Based on the expected higher LVEF range from 17 % to 47 %, the LEF-HG data were further segregated in **Fig. 1B** and **C** into values below (*red*) or above 35% (*black*). (B) Principal component analysis representing single LV biopsy samples from individual patients analyzed by label-free DIA-MS (quantification of 2,273 proteins). Each circle projects individual patient sample data onto component 1 and 2, with the percentage of total variance listed in parentheses (x/y axis legend). Each patient data set is represented by two technical replicates. Circles and labels are colored depending on LVEF values (see blue-to-black LUT inset). Outlying replicates were excluded from this plot (1 NF, 3 LEF-LG, 4 PLF-LG).



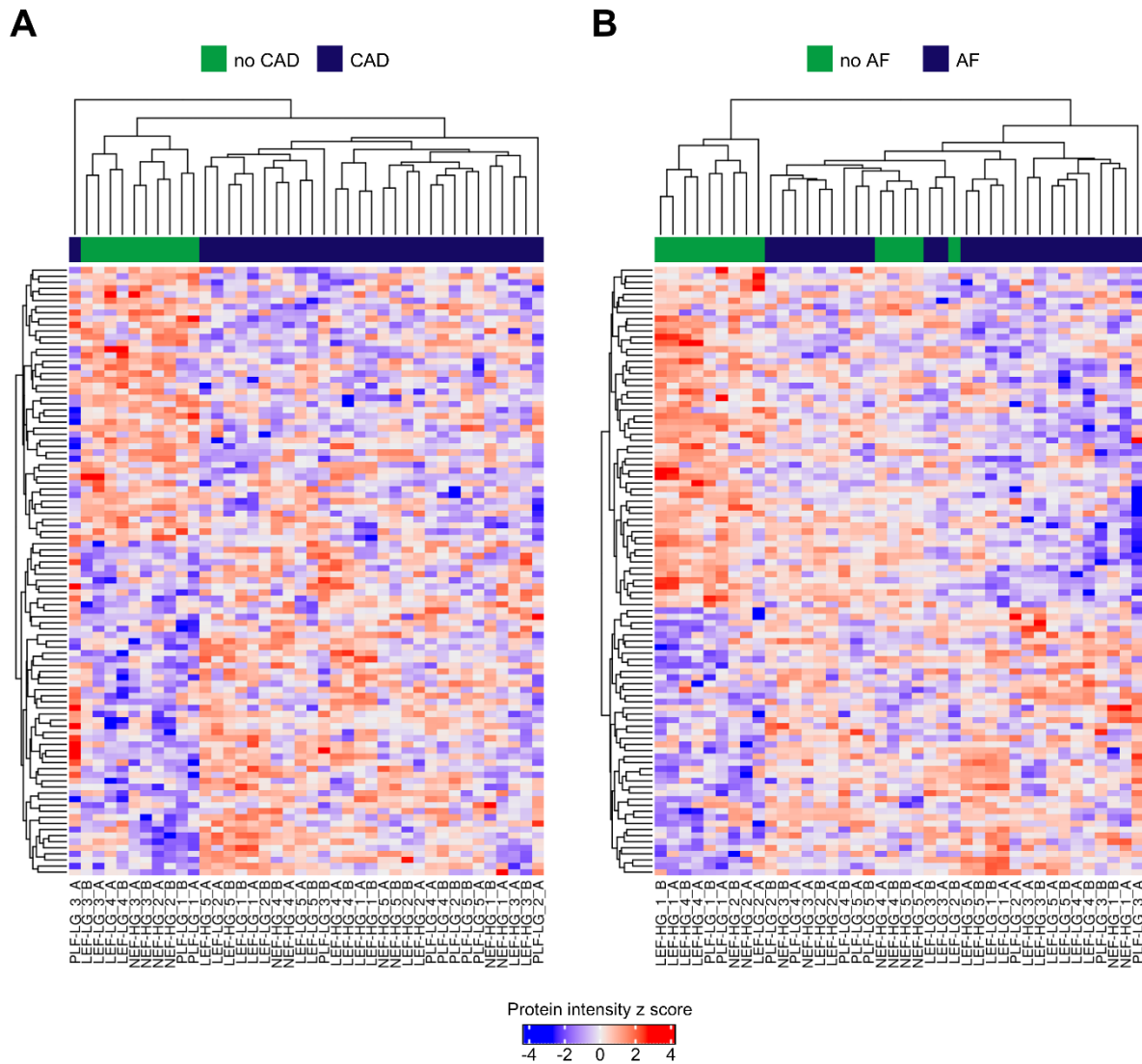
Supplementary Fig. 4. ConsensusClusterPlus. Using hierarchical clustering with complete linkage consensus clusters were constructed. Hierarchical clustering was applied on the normalized DIA-MS data of the 160 differentially abundant proteins. This plot shows the consensus matrices, the CDF of the values in the consensus matrices, relative change in the area under the CDF curves, and the tracking plot of cluster memberships. There is no clear winner. The delta plot suggests no improvement from 9 onwards, but the consensus matrix for 8 clusters does not look clean. The consensus CDF does not reach a flat shape for any of the clusterings. The consensus matrices might suggest 10 clusters including 3 clusters of size 2. Of the clusterings into less clusters, the matrices look relatively clean for 3 or 5 clusters.



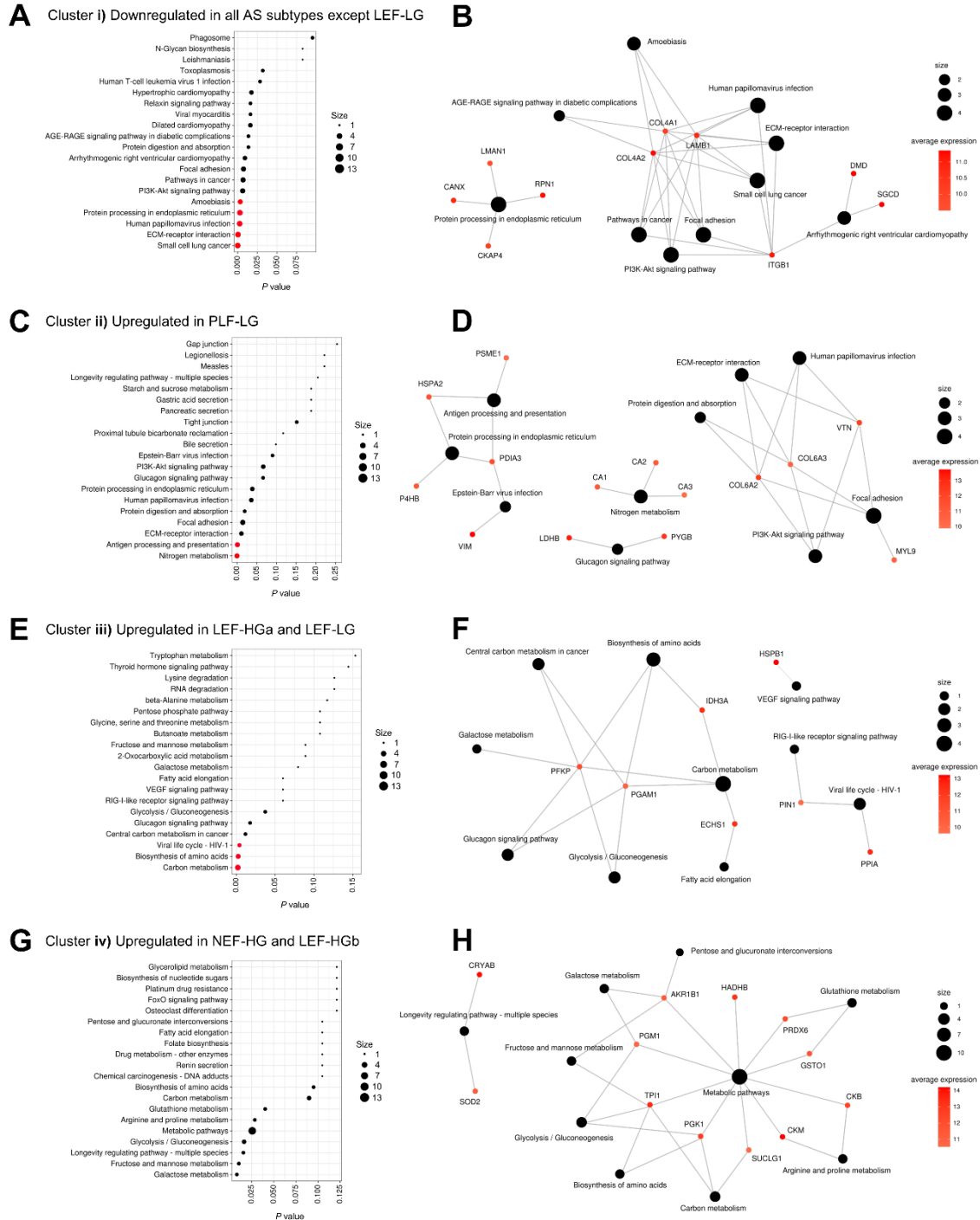
Supplementary Fig. 5. Hierarchical clustering. *Top:* Hubert Statistic to assess the number of clusters in the samples when using the normalized DIA-MS data of the differentially abundant proteins. The Hubert index is a graphical method of determining the number of clusters. In the plot of Hubert index, we seek a significant knee that corresponds to a significant increase of the value of the measure i.e. the significant peak in Hubert index second differences plot. In this case, knees in the Hubert statistic are present for 3, 7, and 11 clusters. *Bottom:* D index to assess the number of clusters in the samples when using the normalized DIA-MS data of the differentially abundant proteins. The D index is a graphical method of determining the number of clusters. In the plot of D index, we seek a significant knee (the significant peak in D index second differences plot) that corresponds to a significant increase of the value of the measure. In this case, the highest peak in D index is visible for 3 clusters.



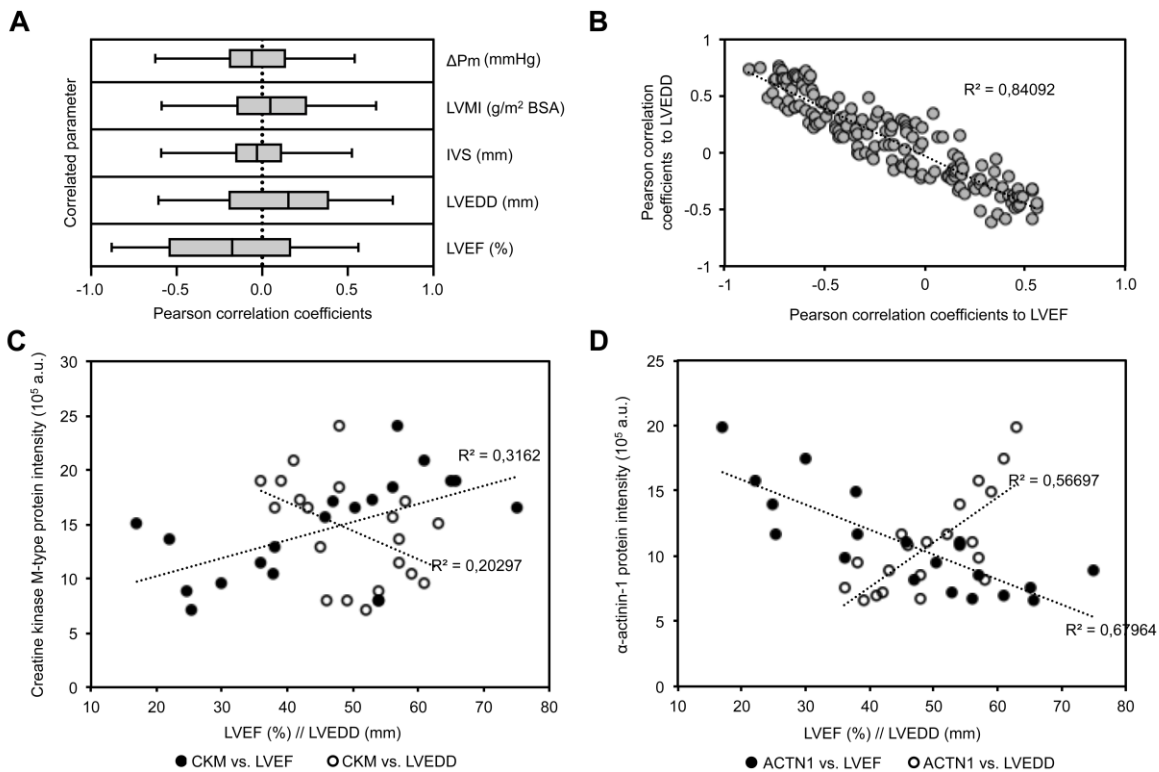
Supplementary Fig. 6. Enriched Gene Ontology terms relative to LEF-LG. Heat map depicting $-\log_{10} P$ values (*top*: look-up-table), sorted according to the highest LEF-LG values. Biological processes/Gene Ontology terms enriched for each AS subtype were compared to NF. Darker colors indicate a higher significance. $n = 5$ biologically independent LV biopsy samples per AS subtype, and 2 technical replicates per patient.



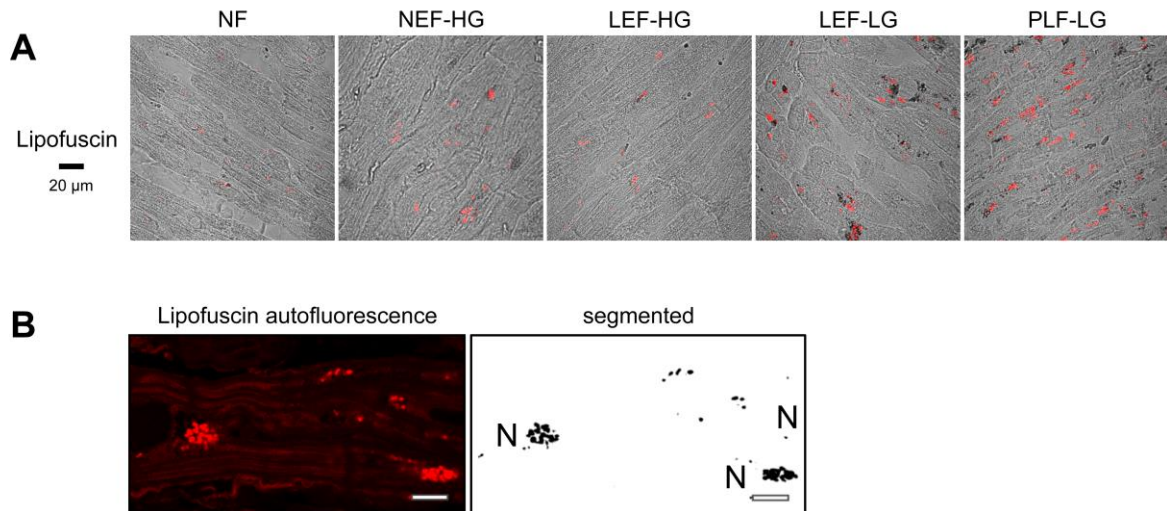
Supplementary Fig. 7. Comorbidities coronary artery disease and atrial fibrillation in AS. Coronary artery disease (CAD) and atrial fibrillation (AF) are frequently observed in AS patients. (A-B) Heat maps for all AS patient biopsies including two technical replicates (A/B) show the abundance of the 100 most regulated proteins in the CAD (*dark blue*) vs. no CAD (*green*) (A), or AF (*dark blue*) vs. no AF (*green*) comparison (B), respectively. After adjusting for multiple testing, none of the quantified proteins remained significantly regulated in the group comparisons.



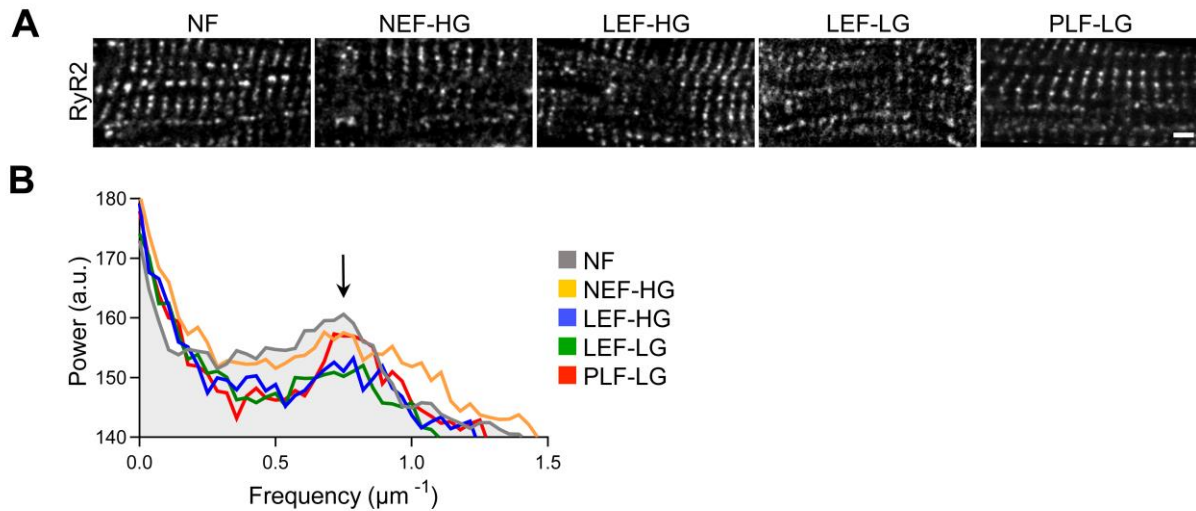
Supplementary Fig. 8. Overrepresented KEGG pathways in clusters i-iv) of Fig. 1C. (A, C, E, G) Top 20 overrepresented KEGG pathways. Red circles indicate KEGG pathways remaining significantly overrepresented after adjusting for multiple testing. (B, D, F, H) Corresponding gene-concept-networks of the top 10 overrepresented KEGG pathways.



Supplementary Fig. 9. Correlation analysis of 160 differentially abundant proteins with left-ventricular echocardiography parameters. (A) Distributions of *Pearson* correlation coefficients between DIA-MS intensity values for 160 differentially abundant proteins and five left-ventricular echocardiography parameters: ΔP_m , aortic valve pressure gradient; IVS, interventricular septum; LVEDD, left-ventricular end-diastolic diameter; LVEF, left-ventricular ejection fraction; LVMI, left-ventricular mass index. Boxes indicate median and interquartile range. (B) *Pearson* correlation coefficients of 160 differential protein abundances versus LVEF (abscissa) and LVEDD (ordinate) confirming a stringent anticorrelation. (C-D) Exemplary correlations of protein abundance values for creatine kinase M-type (CKM, UniProt accession P06732), and α -actinin-1 (ACTN1, UniProt accession P12814-2) versus LVEF and LVEDD, respectively. $n = 5$ LV biopsy samples each for NEF-HG, LEF-HG, LEF-LG and PLF-LG; average DIA-MS intensity values from injection replicates. Please refer to Supplemental Data 2 for detailed data.



Supplementary Fig. 10. Lipofuscin aggregates are increased in aortic stenosis-affected left-ventricular cardiomyocytes. (A) Perinuclear lipofuscin granules (*red*) were visualized by autofluorescence detection upon 405 nm excitation using confocal imaging. Bright field images showing lipofuscin autofluorescent signal spots overlaid on myocardial sections to document intracellular accumulation in cardiomyocytes. (B) *Left*: Confocal lipofuscin autofluorescence signals were predominantly observed in perinuclear granules. *Right*: Image segmentation was used to generate high-contrast data for the signal analysis in **Fig. 4**. N, nucleus. Scale bars 10 μm.



Supplementary Fig. 11. The periodicity of transversal ryanodine receptor type 2 (RyR2) cluster striations is strongly impaired in LEF-HG and LEF-LG. (A) Confocal imaging of immunolabeled RyR2 clusters in longitudinally sectioned LV biopsy samples. Representative images reveal disorganized RyR2 cluster striation signals in LEF-HG and LEF-LG compared to NF biopsy samples. Scale 2 μm , applies to all image panels. (B) Fast *Fourier* transformation [16] power spectra from equally sized (20.45 x 10.23 μm) and longitudinally aligned ROIs of RyR2 confocal images as shown in A. The arrow defines the peak indicating the degree of transversal signal periodicity. n = 5 LV myocytes each of 5/5/5/6/5 biologically independent biopsies.

Variable	NEF-HG	LEF-HG	LEF-LG	PLF-LG	P value (all groups)	P value					
	n=10	n=10	n=10	n=8		I,II	I,III	I,IV	II,III	II,IV	III,IV
Clinical characteristics											
Age (years)	77.50 ± 1.19	77.20 ± 2.91	76.50 ± 2.00	80.25 ± 1.22	0.665	0.999	0.986	0.816	0.995	0.765	0.632
Sex, female, n (%)	3 (30)	3 (30)	1 (10)	3 (38)	0.579	>0.999	0.582	>0.999	0.582	>0.999	0.274
Height (cm)	174.50 ± 2.06	176.40 ± 2.48	176.00 ± 2.37	171.88 ± 3.37	0.663	0.955	0.977	0.908	0.999	0.659	0.721
Weight (kg)	81.10 ± 3.98	91.10 ± 7.93	78.70 ± 4.18	86.38 ± 4.76	0.434	0.606	0.990	0.926	0.427	0.945	0.806
BMI (kg/m ²)	27.23 ± 1.51	29.21 ± 2.46	25.37 ± 1.20	29.39 ± 1.80	0.415	0.876	0.894	0.867	0.475	>0.999	0.487
BSA (m ²)	1.96 ± 0.04	2.06 ± 0.08	1.95 ± 0.06	1.99 ± 0.06	0.617	0.691	0.999	0.985	0.619	0.899	0.967
CAD, n (%)	7 (70)	6 (60)	7 (70)	5 (63)	>0.999	>0.999	>0.999	>0.999	>0.999	>0.999	>0.999
Prior MI, n (%)	1 (10)	1 (10)	2 (20)	1 (13)	>0.999	>0.999	>0.999	>0.999	>0.999	>0.999	>0.999
Prior PCI, n (%)	4 (40)	1 (10)	5 (50)	4 (50)	0.210	0.303	>0.999	>0.999	0.140	0.117	>0.999
Prior CABG, n (%)	1 (10)	1 (10)	0 (0)	0 (0)	>0.999	>0.999	>0.999	>0.999	>0.999	>0.999	>0.999
ICM, n (%)	0 (0)	2 (20)	2 (20)	0 (0)	0.302	0.473	0.473	>0.999	>0.999	0.477	0.477
DCM, n (%)	0 (0)	0 (0)	1 (10)	0 (0)	>0.999	>0.999	>0.999	>0.999	>0.999	>0.999	>0.999
Atrial fibrillation, n (%)	5 (50)	4 (40)	5 (50)	6 (75)	0.548	>0.999	>0.999	0.366	>0.999	0.188	0.366
Peripheral vascular disease, n (%)	5 (50)	3 (30)	3 (30)	2 (25)	0.740	0.649	0.649	0.366	>0.999	>0.999	>0.999
Prior cerebral ischaemia event, n (%)	3 (30)	1 (10)	2 (20)	2 (25)	0.829	0.582	>0.999	>0.999	>0.999	0.558	>0.999
Chronic pulmonary disease, n (%)	1 (10)	1 (10)	3 (30)	2 (25)	0.602	>0.999	0.582	0.558	0.582	0.558	>0.999
Diabetes, n (%)	5 (50)	3 (30)	6 (60)	4 (50)	0.665	0.649	>0.999	>0.999	0.369	0.630	>0.999
CKD (GFR <60 mL/min), n (%)	3 (30)	5 (50)	5 (50)	8 (100)	0.018	0.649	0.649	0.004	>0.999	0.035	0.035
Creatinine (mg/dL)	0.98 ± 0.09	1.14 ± 0.10	1.16 ± 0.12	1.49 ± 0.37	0.353	0.936	0.905	0.287	0.999	0.595	0.648
NT-proBNP (pg/mL)	1331 ± 348	12288 ± 3797	12485 ± 2335	2454 ± 417	0.158	0.302	0.287	0.998	>0.999	0.453	0.436
MLHFQ (points)	22.00 ± 5.23	44.20 ± 5.46	42.90 ± 3.64	44.25 ± 4.61	0.010	0.023	0.035	0.034	0.998	>0.999	0.998
6mwt distance (m)	311.13 ± 28.21	139.67 ± 48.76	190.56 ± 38.04	153.63 ± 48.24	0.048	0.049	0.244	0.093	0.838	0.996	0.935
Echocardiographic parameters											
SWT (mm)	15.80 ± 0.68	14.90 ± 0.50	14.50 ± 0.89	15.50 ± 0.81	0.621	0.830	0.614	0.993	0.981	0.950	0.810
PWT (mm)	15.40 ± 0.75	13.10 ± 0.78	12.80 ± 0.64	14.75 ± 0.55	0.046	0.131	0.071	0.931	0.991	0.437	0.293
LVEDD (mm)	41.80 ± 1.43	56.60 ± 2.59	51.90 ± 1.70	45.50 ± 1.46	<0.001	<0.001	0.004	0.592	0.338	0.003	0.148
LVEDS (mm)	30.90 ± 1.58	47.40 ± 2.98	44 ± 1.56	31.63 ± 2.25	<0.001	<0.001	0.001	0.996	0.707	0.001	0.004
LVEDV (ml)	67.52 ± 6.95	136.05 ± 13.36	125.42 ± 8.77	79.69 ± 12.62	<0.001	0.001	0.003	0.879	0.900	0.008	0.040
LVESV (ml)	27.31 ± 3.67	97.13 ± 12.88	83.26 ± 6.68	32.94 ± 6.20	<0.001	<0.001	0.001	0.971	0.663	<0.001	0.002
LVM (g)	268.80 ± 23.26	362.80 ± 31.54	301.00 ± 23.36	288.38 ± 26.08	0.106	0.088	0.836	0.963	0.388	0.280	0.989
LVMI (g/m ²)	137.86 ± 8.90	179.22 ± 13.84	150.77 ± 10.90	143.89 ± 11.06	0.085	0.079	0.863	0.985	0.331	0.204	0.979
LVEF (%)	60.61 ± 2.12	30.86 ± 3.41	33.93 ± 2.57	58.66 ± 2.20	<0.001	<0.001	<0.001	0.964	0.858	<0.001	<0.001
SVI (ml/m ²)	36.64 ± 2.26	31.44 ± 1.89	29.08 ± 1.66	30.01 ± 0.84	0.035	0.221	0.034	0.103	0.807	0.955	0.987
LVOT (mm)	20.30 ± 0.45	21.10 ± 0.30	22.00 ± 0.65	20.25 ± 0.63	0.097	0.714	0.128	>0.999	0.634	0.713	0.146
AVA (cm ²)	0.61 ± 0.04	0.61 ± 0.04	0.81 ± 0.06	0.75 ± 0.04	0.013	>0.999	0.032	0.260	0.033	0.266	0.826
AVA/BSA (cm ² /m ²)	0.33 ± 0.02	0.31 ± 0.02	0.41 ± 0.03	0.38 ± 0.02	0.008	0.906	0.050	0.467	0.009	0.172	0.707
Vmax (m/s)	4.51 ± 0.12	4.24 ± 0.05	3.15 ± 0.11	3.39 ± 0.09	<0.001	0.243	<0.001	<0.001	<0.001	<0.001	0.390
ΔPm (mmHg)	49.20 ± 3.36	43.60 ± 0.81	23.70 ± 1.78	26.38 ± 1.73	<0.001	0.305	<0.001	<0.001	<0.001	<0.001	0.855

Supplementary Table 1. Clinical characteristics and pre-interventional echocardiographic parameters from patients with left-ventricular biopsy samples analyzed by DIA-MS and superresolution STED microscopy. 6mwt, 6 min walk test; AVA, aortic valve area; BMI, body mass index; BSA, body surface area; CABG, coronary artery bypass grafting; CAD, coronary artery disease; CKD, chronic kidney disease; DCM, dilative cardiomyopathy; ΔPm, aortic valve pressure gradient; ICM, ischemic cardiomyopathy; LVEDD, left-ventricular end-diastolic diameter; LVEDV, left-ventricular end-diastolic volume; LVEF, left-ventricular ejection fraction; LVESD, left-ventricular end-systolic diameter; LVESV, left-ventricular end-systolic volume; LVM, left-ventricular mass; LVMI, left-ventricular mass index; LVOT, left-ventricular outflow tract; MI, myocardial infarction; MLHFQ, Minnesota living with heart failure quality of life questionnaire; PCI, percutaneous coronary intervention; PWT, posterior wall thickness; SVI, stroke volume index; SWT, septal wall thickness; Vmax, peak aortic valve velocity. Comparison of all four groups: one-way ANOVA for continuous variables and the Fisher's exact test for categorical variables. Two group comparisons: post-hoc Tukey test for continuous variables and the Fisher's exact test for categorical variables. *P* values < 0.05 are highlighted in bold.

Variable	NEF-HG n=5	LEF-HG n=5	LEF-LG n=5	PLF-LG n=5
Clinical characteristics				
Age (years)	78.60 ± 2.05	74.60 ± 4.13	78.40 ± 3.07	79.80 ± 1.21
Sex, female, n (%)	2 (40)	1 (20)	0 (0)	2 (40)
Height (cm)	171.80 ± 2.83	175.60 ± 1.91	176.40 ± 3	172.00 ± 5.37
Weight (kg)	85.80 ± 5.60	103.00 ± 10.87	81.20 ± 5.16	82.20 ± 5.65
BMI (kg/m ²)	30.18 ± 1.96	33.40 ± 3.54	26.06 ± 1.37	28.02 ± 2.32
BSA (m ²)	1.98 ± 0.05	2.17 ± 0.10	1.98 ± 0.08	1.96 ± 0.09
CAD, n (%)	3 (60)	5 (100)	3 (60)	4 (80)
Prior MI, n (%)	1 (20)	1 (20)	1 (20)	1 (20)
Prior PCI, n (%)	2 (40)	1 (20)	3 (60)	3 (60)
Prior CABG, n (%)	0 (0)	1 (20)	0 (0)	0 (0)
ICM, n (%)	0 (0)	2 (40)	1 (20)	0 (0)
DCM, n (%)	0 (0)	0 (0)	1 (20)	0 (0)
Atrial fibrillation, n (%)	2 (40)	3 (60)	4 (80)	4 (80)
Peripheral vascular disease, n (%)	2 (40)	3 (60)	2 (40)	1 (20)
Prior cerebral ischaemia event, n (%)	2 (40)	1 (20)	0 (0)	2 (40)
Chronic pulmonary disease, n (%)	1 (20)	1 (20)	0 (0)	2 (40)
Diabetes, n (%)	3 (60)	2 (40)	3 (60)	2 (40)
CKD (GFR <60 mL/min), n (%)	0 (0)	4 (80)	3 (60)	5 (100)
Creatinine (mg/dL)	0.85 ± 0.10	1.34 ± 0.14	1.18 ± 0.16	1.85 ± 0.53
NT-proBNP (pg/mL)	1758 ± 655	10745 ± 4301	16356 ± 12013	2269 ± 554
MLHFQ (points)	18.20 ± 4.45	46.00 ± 8.99	48.20 ± 5.71	48.00 ± 6.01
6mwt distance (m)	299.75 ± 17.43	141.25 ± 72.36	188.00 ± 48.33	107.00 ± 64.54
Echocardiographic parameters				
SWT (mm)	17.40 ± 0.61	16.00 ± 0.49	14.80 ± 1.00	14.20 ± 0.52
PWT (mm)	17.20 ± 0.91	12.80 ± 1.00	12.20 ± 0.59	14.00 ± 0.49
LVEDD (mm)	41.40 ± 2.01	59.00 ± 1.17	53.40 ± 2.17	44.60 ± 1.59
LVEDS (mm)	31.40 ± 1.43	47.80 ± 3.20	46.20 ± 2.55	30.80 ± 3.36
LVEDV (ml)	71.16 ± 10.45	147.64 ± 20.18	139.70 ± 10.70	57.96 ± 6.16
LVESV (ml)	28.42 ± 5.69	104.14 ± 20.16	94.12 ± 6.92	35.60 ± 9.42
LVM (g)	311.40 ± 31.99	392.20 ± 9.67	309.00 ± 28.53	248.00 ± 12.54
LVMI (g/m ²)	155.66 ± 12.10	190.05 ± 10.85	150.92 ± 12.83	128.02 ± 8.07
LVEF (%)	61.08 ± 3.86	32.36 ± 5.45	32.38 ± 2.70	57.10 ± 2.02
SVI (ml/m ²)	35.69 ± 3.27	30.74 ± 2.16	29.85 ± 2.24	29.46 ± 0.98
LVOT (mm)	19.60 ± 0.22	20.60 ± 0.22	22.80 ± 0.77	19.80 ± 0.59
AVA (cm ²)	0.60 ± 0.05	0.60 ± 0.05	0.81 ± 0.08	0.78 ± 0.05
AVA/BSA (cm ² /m ²)	0.31 ± 0.03	0.29 ± 0.02	0.41 ± 0.04	0.40 ± 0.03
Vmax (m/s)	4.67 ± 0.18	4.16 ± 0.04	3.08 ± 0.17	3.34 ± 0.13
ΔPm (mmHg)	53.40 ± 4.18	53.40 ± 4.18	23.00 ± 2.64	23.80 ± 1.91

Supplementary Table 2. Clinical characteristics and pre-interventional echocardiographic parameters from patients with proteomically analyzed left-ventricular biopsy samples for DIA-MS. 6mwt, 6 min walking test; AVA, aortic valve area; BMI, body mass index; BSA, body surface area; CABG, coronary artery bypass grafting; CAD, coronary artery disease; CKD, chronic kidney disease; DCM, dilative cardiomyopathy; ΔPm, aortic valve pressure gradient; ICM, ischemic cardiomyopathy; LVEDD, left-ventricular end-diastolic diameter; LVEDV, left-ventricular end-diastolic volume; LVEF, left-ventricular ejection fraction; LVESD, left-ventricular end-systolic diameter; LVESV, left-ventricular end-systolic volume; LVM, left-ventricular mass; LVMI, left-ventricular mass index; LVOT, left-ventricular outflow tract; MI, myocardial infarction; MLHFQ, Minnesota living with heart failure quality of life questionnaire; PCI, percutaneous coronary intervention; PWT, posterior wall thickness; SVI, stroke volume index; SWT, septal wall thickness; Vmax, peak aortic valve velocity.

Variable	NEF-HG n=5	LEF-HG n=5	LEF-LG n=6	PLF-LG n=5
Clinical characteristics				
Age (years)	76.40 ± 2.66	79.80 ± 3.75	76.67 ± 2.66	80.40 ± 1.69
Sex, female, n (%)	1 (20)	2 (40)	1 (17)	2 (40)
Height (cm)	177.20 ± 2.46	177.20 ± 4.56	174.60 ± 3.16	170.00 ± 1.62
Weight (kg)	76.40 ± 4.80	79.20 ± 8.75	74.67 ± 5.51	90.60 ± 5.79
BMI (kg/m ²)	24.28 ± 1.32	25.01 ± 2.15	24.43 ± 1.62	31.46 ± 2.29
BSA (m ²)	1.93 ± 0.07	1.96 ± 0.12	1.89 ± 0.07	2.02 ± 0.05
CAD, n (%)	4 (80)	1 (20)	4 (67)	3 (60)
Prior MI, n (%)	0 (0)	0 (0)	1 (17)	0 (0)
Prior PCI, n (%)	2 (40)	0 (0)	3 (50)	2 (40)
Prior CABG, n (%)	1 (20)	0 (0)	0 (0)	0 (0)
ICM, n (%)	0 (0)	0 (0)	1 (17)	0 (0)
DCM, n (%)	0 (0)	0 (0)	0 (0)	0 (0)
Atrial fibrillation, n (%)	3 (60)	1 (20)	2 (33)	4 (80)
Peripheral vascular disease, n (%)	3 (60)	0 (0)	0 (0)	1 (20)
Prior cerebral ischaemia event, n (%)	1 (20)	0 (0)	1 (17)	2 (40)
Chronic pulmonary disease, n (%)	0 (0)	0 (0)	0 (0)	1 (20)
Diabetes, n (%)	2 (40)	1 (20)	2 (33)	3 (60)
CKD (GFR <60 mL/min), n (%)	3 (60)	1 (20)	1 (17)	5 (100)
Creatinine (mg/dL)	1.12 ± 0.13	0.93 ± 0.07	1.05 ± 0.14	1.74 ± 0.56
NT-proBNP (pg/mL)	989 ± 256	13523 ± 5848	6581 ± 2652	2784 ± 485
MLHFQ (points)	25.80 ± 9.16	42.40 ± 6.10	37.83 ± 5.24	47.60 ± 6.25
6mwt distance (m)	322.50 ± 53.05	138.40 ± 65.96	202.00 ± 47.06	152.60 ± 50.87
Echocardiographic parameters				
SWT (mm)	14.20 ± 0.66	13.80 ± 0.52	14.17 ± 1.21	16.60 ± 0.92
PWT (mm)	13.60 ± 0.36	13.40 ± 1.19	13.33 ± 0.90	15.60 ± 0.61
LVEDD (mm)	42.20 ± 2.01	54.20 ± 4.80	49.50 ± 2.20	45.60 ± 2.17
LVESD (mm)	30.40 ± 3.14	47.00 ± 5.60	41.67 ± 1.02	30.80 ± 3.40
LVEDV (ml)	63.88 ± 8.88	124.46 ± 15.91	114.03 ± 9.19	89.78 ± 18.08
LVESV (ml)	26.21 ± 4.60	90.12 ± 15.39	73.60 ± 7.69	35.60 ± 9.42
LVM (g)	226.20 ± 20.36	333.40 ± 59.50	283.33 ± 31.79	318.40 ± 34.39
LVMi (g/m ²)	120.05 ± 6.55	168.38 ± 24.52	147.55 ± 14.96	155.06 ± 13.62
LVEF (%)	60.14 ± 1.72	29.36 ± 3.98	35.92 ± 3.57	61.28 ± 2.92
SVI (ml/m ²)	37.58 ± 3.06	32.15 ± 3.06	27.41 ± 2.18	30.55 ± 1.12
LVOT (mm)	21.00 ± 0.75	21.60 ± 0.46	21.00 ± 0.78	20.60 ± 0.78
AVA (cm ²)	0.62 ± 0.06	0.62 ± 0.06	0.75 ± 0.09	0.77 ± 0.06
AVA/BSA (cm ² /m ²)	0.35 ± 0.01	0.32 ± 0.03	0.39 ± 0.04	0.39 ± 0.03
Vmax (m/s)	4.35 ± 0.14	4.32 ± 0.09	3.29 ± 0.12	3.33 ± 0.11
ΔPm (mmHg)	45.00 ± 4.53	44.20 ± 1.37	24.67 ± 1.98	27.20 ± 2.20

Supplementary Table 3. Clinical characteristics and pre-interventional echocardiographic parameters from patients with left-ventricular biopsy samples analyzed by superresolution STED microscopy. 6mwt, 6 min walking test; AVA, aortic valve area; BMI, body mass index; BSA, body surface area; CABG, coronary artery bypass grafting; CAD, coronary artery disease; CKD, chronic kidney disease; DCM, dilative cardiomyopathy; ΔPm, aortic valve pressure gradient; ICM, ischemic cardiomyopathy; LVEDD, left-ventricular end-diastolic diameter; LVESD, left-ventricular end-systolic diameter; LVEDV, left-ventricular end-diastolic volume; LVEF, left-ventricular ejection fraction; LVESV, left-ventricular end-systolic volume; LVM, left-ventricular mass; LVMi, left-ventricular mass index; LVOT, left-ventricular outflow tract; MI, myocardial infarction; MLHFQ, Minnesota living with heart failure quality of life questionnaire; PCI, percutaneous coronary intervention; PWT, posterior wall thickness; SVI, stroke volume index; SWT, septal wall thickness; Vmax, peak aortic valve velocity.

Index	No. of clusters
frey	1
mcclain	2
cindex	4
silhouette	2
dunn	15
kl	4
ch	2
hartigan	3
db	6
duda	4
pseudot2	4
beale	4
ratkowsky	3
ball	3
ptbiserial	5
gap	2
gamma	15
gplus	15
tau	3
hubert	3
hubert	7
hubert	11
sdindex	6
dindex	3
sdbw	15

No. of clusters	n
1	1
2	4
3	6
4	5
5	1
6	2
7	1
11	1
15	4

Supplementary Table 4. Hierarchical clustering. Assessment of the number of clusters in patient LV biopsies when using the normalized DIA-MS data of the 160 differentially abundant proteins. Clusterings into 2 - 15 clusters were assessed using different indices. The left table shows for each index the number of clusters that is suggested by the index. The right table shows for each number of clusters the number of indices that suggest that number of clusters.

References

- [1] T. Guo, P. Kouvonen, C.C. Koh, L.C. Gillet, W.E. Wolski, H.L. Rost, G. Rosenberger, B.C. Collins, L.C. Blum, S. Gillessen, M. Joerger, W. Jochum, R. Aebersold, Rapid mass spectrometric conversion of tissue biopsy samples into permanent quantitative digital proteome maps, *Nat Med* 21(4) (2015) 407-13.
- [2] H. Stephanowitz, S. Lange, D. Lang, C. Freund, E. Krause, Improved two-dimensional reversed phase-reversed phase LC-MS/MS approach for identification of peptide-protein interactions, *J Proteome Res* 11(2) (2012) 1175-83.
- [3] G. Losensky, K. Jung, H. Urlaub, F. Pfeifer, S. Frols, C. Lenz, Shedding light on biofilm formation of *Halobacterium salinarum* R1 by SWATH-LC/MS/MS analysis of planktonic and sessile cells, *Proteomics* 17(7) (2017).
- [4] Y. Zhang, A. Bilbao, T. Bruderer, J. Luban, C. Strambio-De-Castillia, F. Lisacek, G. Hopfgartner, E. Varesio, The Use of Variable Q1 Isolation Windows Improves Selectivity in LC-SWATH-MS Acquisition, *J Proteome Res* 14(10) (2015) 4359-71.
- [5] J.P. Lambert, G. Ivosev, A.L. Couzens, B. Larsen, M. Taipale, Z.Y. Lin, Q. Zhong, S. Lindquist, M. Vidal, R. Aebersold, T. Pawson, R. Bonner, S. Tate, A.C. Gingras, Mapping differential interactomes by affinity purification coupled with data-independent mass spectrometry acquisition, *Nat Methods* 10(12) (2013) 1239-45.
- [6] M.E. Ritchie, B. Phipson, D. Wu, Y. Hu, C.W. Law, W. Shi, G.K. Smyth, limma powers differential expression analyses for RNA-sequencing and microarray studies, *Nucleic Acids Res* 43(7) (2015) e47.
- [7] G.K. Smyth, J. Michaud, H.S. Scott, Use of within-array replicate spots for assessing differential expression in microarray experiments, *Bioinformatics* 21(9) (2005) 2067-75.
- [8] M.D. Wilkerson, D.N. Hayes, ConsensusClusterPlus: a class discovery tool with confidence assessments and item tracking, *Bioinformatics* 26(12) (2010) 1572-3.
- [9] G. Yu, L.G. Wang, Y. Han, Q.Y. He, clusterProfiler: an R package for comparing biological themes among gene clusters, *OMICS* 16(5) (2012) 284-7.
- [10] S. Brandenburg, J. Pawlowitz, F.E. Fakuade, D. Kownatzki-Danger, T. Kohl, G.Y. Mitronova, M. Scardigli, J. Neef, C. Schmidt, F. Wiedmann, F.S. Pavone, L. Sacconi, I. Kutschka, S. Sossalla, T. Moser, N. Voigt, S.E. Lehnart, Axial Tubule Junctions Activate Atrial Ca(2+) Release Across Species, *Front Physiol* 9 (2018) 1227.
- [11] E. Wagner, S. Brandenburg, T. Kohl, S.E. Lehnart, Analysis of tubular membrane networks in cardiac myocytes from atria and ventricles, *J Vis Exp* (92) (2014) e51823.
- [12] S. Brandenburg, J. Pawlowitz, B. Eikenbusch, J. Peper, T. Kohl, G.Y. Mitronova, S. Sossalla, G. Hasenfuss, X.H. Wehrens, P. Kohl, E.A. Rog-Zielinska, S.E. Lehnart, Junctophilin-2 expression rescues atrial dysfunction through polyadic junctional membrane complex biogenesis, *JCI Insight* 4(12) (2019).
- [13] D. Baddeley, I.D. Jayasinghe, L. Lam, S. Rossberger, M.B. Cannell, C. Soeller, Optical single-channel resolution imaging of the ryanodine receptor distribution in rat cardiac myocytes, *Proc Natl Acad Sci U S A* 106(52) (2009) 22275-80.
- [14] R. Carroll, D. Ruppert, L. Stefanski, C. Crainiceanu, *Measurement Error in Nonlinear Models: A Modern Perspective*, Chapman and Hall (2006).
- [15] J.R. Cook, L.A. Stefanski, Simulation-extrapolation estimation in parametric measurement error models, *Journal of the American Statistical Association* 89 (1994) 1314-1328.
- [16] E.C. Arakel, S. Brandenburg, K. Uchida, H. Zhang, Y.W. Lin, T. Kohl, B. Schrul, M.S. Sulkin, I.R. Efimov, C.G. Nichols, S.E. Lehnart, B. Schwappach, Tuning the electrical properties of the heart by differential trafficking of KATP ion channel complexes, *J Cell Sci* 127(Pt 9) (2014) 2106-19.